Solving the Scattering Problem for the P3HT On-Chain Charge Transport

A. Lücke, U. Gerstmann, S. Sanna, M. Landmann, A. Riefer, M. Rohrmüller, N.J. Vollmers, M. Witte, E. Rauls, R. Hölscher, C. Braun, S. Neufeld, K. Holtgrewe, and W.G. Schmidt

Abstract The effect of oxygen impurities and structural imperfections on the coherent on-chain quantum conductance of poly(3-hexylthiophene) is calculated from *first principles* by solving the scattering problem for molecular structures obtained within density functional theory. It is found that the conductance drops substantially for polymer kinks with curvature radii smaller than 17 Å and rotations in excess of about 60°. Oxidation of thiophene group carbon atoms drastically reduces the conductance, whereas the oxidation of the molecular sulfur barely changes the coherent transport properties. Also isomer defects in the coupling along the chain direction are of minor importance for the intrachain transmission.

1 Introduction

Organic semiconductors are increasingly used for a wide range of devices ranging from organic light-emitting diodes and transistors to organic solar cells. In particular their low cost fabrication processes and the possibility to fine-tune desired functions by chemical modification of their building blocks make them interesting for numerous applications. Poly(3-hexylthiophene-2,5-diyl) also known as P3HT is one of the most important examples for organic semiconductors [1]. It is a *p* conducting organic polymer that is frequently used as active layer in organic solar cells as well as for organic field-effect transistors. Previous studies on the electronic properties concluded that the molecular electron and hole wave functions are delocalized over several thiophene rings and become spatially confined due to ring torsions and chain bendings [2–4] as well as fluctuations of the electrostatic potential caused by adjacent polymer chains [5]. Furthermore it was reported that defects like kinks or torsions do not result in a significant localization of the excited states[6]. There are various publications that address the P3HT transport properties: Improved transport properties for higher molecular weight (MW) chains are reported

A. Lücke • U. Gerstmann • S. Sanna, M. Landmann • A. Riefer • M. Rohrmüller • N.J. Vollmers • M. Witte • E. Rauls • R. Hölscher • C. Braun • S. Neufeld • K. Holtgrewe • W.G. Schmidt (✉)
Lehrstuhl für Theoretische Physik, Universität Paderborn, 33095 Paderborn, Germany
e-mail: W.G.Schmidt@upb.de

W.E. Nagel et al. (eds.), *High Performance Computing in Science and Engineering '15*, DOI 10.1007/978-3-319-24633-8_10

in [7–10] and rationalized by band transport in high MW films composed of long polymer chains, while hopping processes dominate in low MW polymer films. However, it was noted that using processing conditions which allow the chains to equilibrate, increases the mobility even in low MW P3HT [11]. The electron transport in high MW polycrystalline P3HT films was found to be highly anisotropic, with larger mobilities along the chains than perpendicular, i.e., parallel to the stacking direction [12]. These findings are in accordance with transfer integral calculations [13, 14] that find the intrachain direction to be the dominating charge-transport route within P3HT ordered domains [15].

Previous theoretical studies like transfer integral calculations have contributed much to the qualitative understanding of the P3HT electron transport properties. Quantitative data on the modification of the P3HT quantum conductance upon structural or chemical modification are not available yet, however. This concerns, for example, the oxygen-related degradation of the transport properties. The present study is a first step in that direction. The P3HT potential energy surface depends critically on the side chains and cannot be simply derived from smaller systems such as bithiophene [16], which may significantly influence the calculated transport properties due to the sensitivity of the transfer integrals [13, 17, 18]. Also isomeric dispersion may be important [19]. Therefore, much attention is paid here to the realistic modelling of the molecular geometry and the accurate solution of the scattering problem [20] based on the electron structure obtained within density functional theory. On the other hand, our study focusses on single polymer chains, is restricted to the ballistic limit and neglects temperature effects [21]. These are clearly highly idealized conditions. Still, information on coherent on-chain transport is essential for understanding transport characteristics in real samples, in particular since transport in bulk P3HT is largely influenced by tie molecules spanning adjacent nanocrystalline lamellae [12].

2 Methodology

The present calculations are based on density functional theory (DFT) as implemented in the QUANTUM-ESPRESSO-package [22]. Infinite molecular chains are modeled by a supercell approach with periodic boundary conditions. Ultrasoft pseudopotentials [23] in Kleinman-Bylander form [24] are used to model the ion-electron interaction. The electronic many-body interactions are described in generalized gradient approximation (GGA) using the PBE functional [25, 26]. Dispersion interaction is taken into account by the so-called DFT-D approach, i.e., by a semi-empirical London-type correction term [27, 28] using parameters suggested by Grimme [29]. Plane waves up to an energy cutoff of 544 eV are used as basis set for the expansion of the electron wave functions.

The ballistic conductance is obtained from the solution of the scattering problem as outlined by Choi et al. [30] and Smogunov et al. [31]. For the actual calculations we use the PWCOND program [32] that has been modified in our group for better

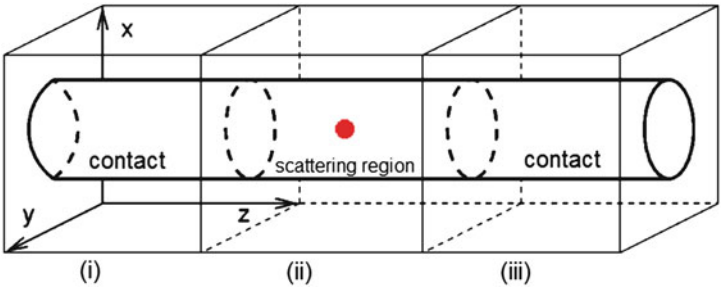

Fig. 1 Schematic setup of the scattering region that contains the investigated defect and is sandwiched between two ideal, semi-infinite contacts

performance on parallel architectures. Below we first outline the methodology and then our modifications to the code that were made for better scalability.

In order to determine the on-chain transmission of charge carriers with energy E through a defect we divide the system along the z direction into three regions as shown schematically in Fig. 1. The left and right contact (i) and (iii), respectively, are assumed to be ideal without any defects and the scattering region (ii) contains the defect. As the influence of the defect on the electronic structure may extend along the polymer chain, parts of the intact molecule should be included into the scattering region. The calculation then proceeds as follows:

1. The total electron potential for regions (i), (ii), and (iii) is obtained self-consistently within DFT for each region separately using periodic boundary conditions. Thereby infinite polymer chains serve as contacts. The scattering region around the defect must be sufficiently large to ensure a smooth match of the potentials.
2. Based on the total potential for each region the electron wave functions are determined without specifying any boundary conditions for the $z = 0$ and $z = L_z$ plane (where L_z is the length of the actual region). These boundary conditions are introduced in the next steps when we calculate the propagating modes in the contacts and the transmission through the whole system. Because of the open boundaries we can find a set of wavefunctions that are parametrized in the form $\Psi = \sum_n a_n \psi_n$. This is done separately for each of the three regions using as many free parameters a_n as the number of open boundary conditions.
3. The propagating ($\Im(k_z) = 0$) and evanescent ($\Im(k_z) \neq 0$) modes (in z-direction) in the contacts are determined exploiting Bloch's theorem for the periodically repeated potential of the contacts, i.e.,

$$\Psi_{k_z}(L_z) = e^{ik_z L_z} \Psi_{k_z}(0). \tag{1}$$

This represents a generalized eigenvalue problem for the eigenvalues $e^{ik_z L_z}$, where the eigenvectors are given by the free parameters a_{n,k_z} in $\Psi_{k_z} = \sum_n a_{n,k_z} \psi_n$ (cf. step 2). It is solved with the `LAPACK` routine `ZGGEV`.

4. The results of the previous steps enter the ansatz below that describes the electron wave function in the three regions as

$$\Psi = \begin{cases} \Psi_{k_z} + \sum\limits_{\Im(k'_z)\leq 0} r_{k_z,k'_z}\Psi_{k'_z} & z \text{ in I} \\ \sum\limits_{n} a_n \Psi_n & z \text{ in II} \\ \sum\limits_{\Im(k'_z)\geq 0} t_{k_z,k'_z}\Psi_{k'_z} & z \text{ in III,} \end{cases} \tag{2}$$

   and which is solved for the coefficients r_{k_z,k'_z}, a_n and t_{k_z,k'_z} that describe k_z modes that propagate to the right hand side with energy E in the left contact ($\Im(k_z) = 0$, $\Re(k_z) > 0$). Thereby the `LAPACK` routine `ZGESV` is utilized.
5. Finally, the quantum conductance $G(E)$ is calculated from the coefficients t_{k_z,k'_z} weighted with the probability current I_{k_z} of the corresponding k_z mode

$$G(E) = \frac{2e^2}{h} \sum_{k_z} \frac{1}{I_{k_z}} \sum_{k'_z} I_{k'_z} |t_{k_z,k'_z}|^2. \tag{3}$$

   In order to obtain the conductance at further charge carrier energies the calculations above are repeated for different values of E starting at step 2. Eventually, the quantum conductance as function of the charge carrier energy $G(E)$ is obtained.

In the original `PWCOND` code the calculation of the set of wavefunctions in step 2 is parallelized over the number of FFT grid points in z direction. Thereby each MPI process calculates the wavefunction in its own subregion. The wavefunctions for the full region are afterwards determined by matching the boundary conditions between the subregions of the single processes. The corresponding data collection is done in a tree-like manner with a depth proportional to the logarithm of the number of subregions, cf. Fig. 2. This procedure is applied to each of the three regions (i), (ii), and (iii) in Fig. 1. Afterwards steps 3 and 4 of the algorithm above are performed in serial calculations. This is acceptable for systems, which mainly extend in z direction, but are small along x and y: Since the matrices in step 3 and 4 scale with the number of grid points perpendicular to the transport direction, the computational effort for steps 3 and 4 is far smaller than for step 2 in such cases. The P3HT polymer studied here, however, does not have a large aspect ratio due to its long hexyl side chains. Therefore its transport characteristics are not efficiently obtained using the existing parallelization scheme of `PWCOND`.

In order to make this system tractable, we therefore parallelized steps 3 and 4 of the algorithm above. Thereby it is exploited that the transmission for charge carriers with energy E can be calculated independently from the ones with energy E'. Therefore almost linear scaling is achieved by implementing parallelization over the charge carrier energies E which allows for determining the transmission $G(E)$ for the complete energy window. The speed-up depends obviously on the energy

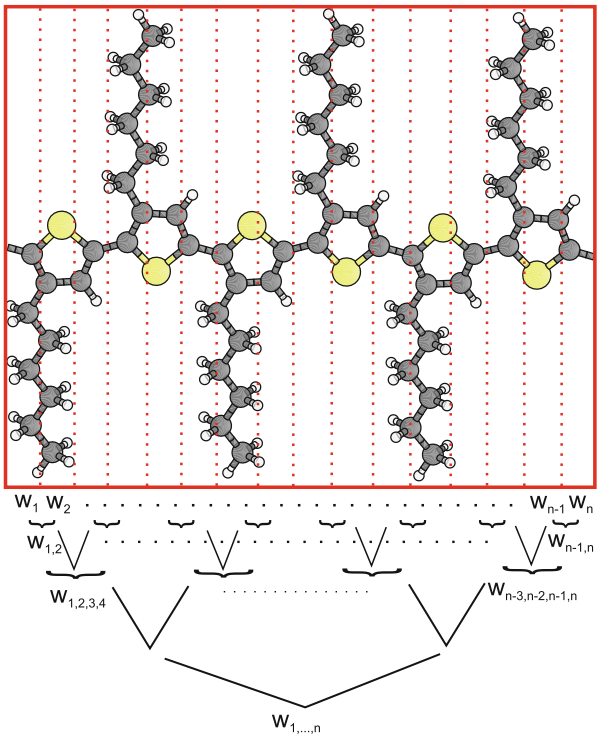

Fig. 2 Illustration of the load distribution (see text) onto several parallel processes and the tree-like access to single subregions exemplarily shown for P3HT contact calculations

region considered, but typically is of the order of two or three orders of magnitude in wall-clock time.

Additionally, we improve the efficiency of the calculations by modifying the numerical implementation of the boundary conditions between the scatter region (ii) and the contacts (i) and (iii) in `PWCOND`: We perform self-consistent electronic structure calculations for an extended scattering region and reduce its size afterwards for solving the scattering problem. This modification of the `PWCOND` module is not only useful to cut computational effort, it is also indispensable for systems where the scattering region is not periodic. It thus allows to overcome the limitations of the periodic boundary conditions for systems that have no corresponding translational symmetry. For a detailed description of these modifications and the corresponding test calculations we refer the reader to [33].

Altogether, we modified the `PWCOND` code in such a way that it may be used for the accurate solution of the scattering problem for large systems containing several hundred atoms. Thus the quantum conductance of real polymers containing structural and chemical defects (see, e.g., Fig. 3 for an example considered here) is accessible to parameter-free electronic structure calculations. The conductance of

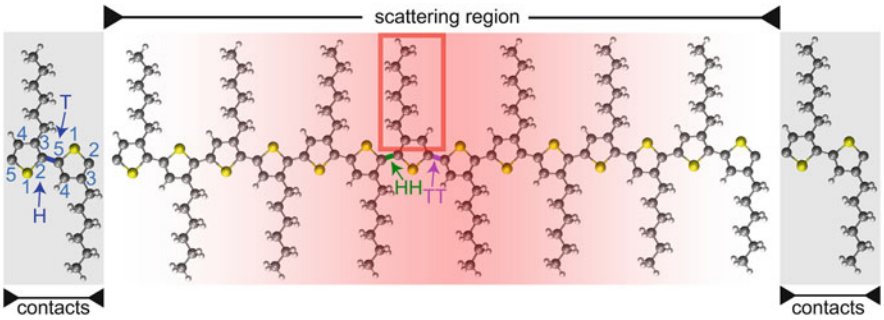

Fig. 3 Schematic setup of the transport calculations, exemplarily shown for the case of isomer defects: the scatter region contains the investigated defect consisting of a HH-TT linkage between the thiophene rings which is caused by a swapped position of the hexyl side chain (*red rectangle*). The contacts are made of ideal rr-HT-P3HT. In the *left* contact modeled by two monomers the atomic numbering is indicated. *H* denotes the second and *T* the fifth position

systems such as studied here that are modelled with about 400 atoms can presently be obtained within about 10 h wall-clock time using 1024 cores on the HLRS Cray XC40. We are presently working on further improving the scaling behaviour of the code by using `ScaLAPACK` routines for the matrix operations.

From a physics point of view, however, it has to be said the present approach still neglects bias voltage and dissipative scattering effects.While this should not affect qualitative trends with respect to the influence of, e.g., structural deformations on the conductance which we investigate here, it restricts meaningful quantitative predictions to conditions of small bias and low temperature. The present calculations model the contacts by ideal P3HT polymers, cf. Fig. 3, which have strongly dispersive and well separated valence bands. Hence *p* conductance suppressing bias voltage effects can be expected to be small.

3 Results and Discussion

P3HT polymer chains are characterized by large carrier mobilities ($\sim 10^3\,\mathrm{cm}^2/\mathrm{Vs}$) [34] which may re reduced, however, due to conformational modifications likely to occur in actual blends [35, 36] as well as oxygen impurities due to, e.g., exposure to ambient conditions [37].

In the following the effect of a twist of the P3HT chains—as shown in Fig. 4—on its quantum conductance is studied. The scattering region considered here consists of 12 monomers. The atoms of the two outer monomers on each side are kept fixed during the relaxation. Since the present calculations employ periodic boundary conditions, two additional monomers are added on each side to decouple the torsion from its periodic images. The total region contains about 400 atoms within a cell that is about 63 Å long. After the electron structure of this system has been

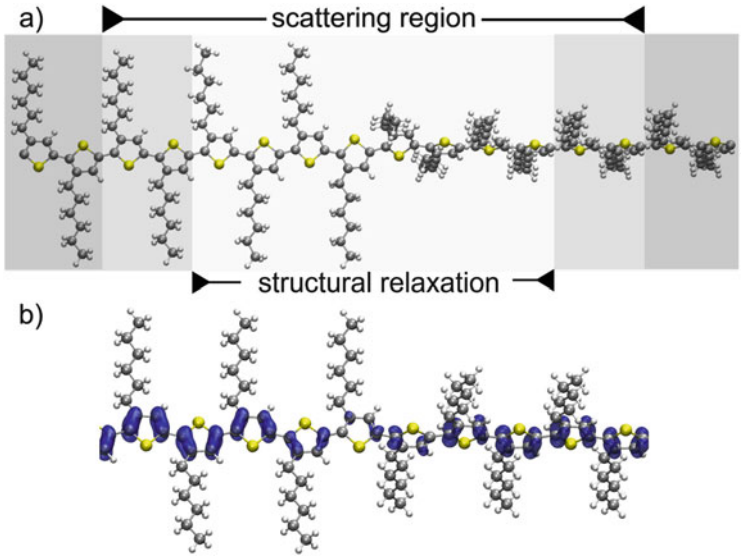

Fig. 4 (**a**) Schematic setup used to describe the electron transport across a chain torsion. The atoms of the outer four monomers of the scattering region are kept frozen during structural relaxation. Additional four monomers outside the scattering region decouple the torsion from its periodic images. (**b**) Charge density isosurfaces indicate the HOMO of a structure with a 90° torsion between two thiophene rings

determined self-consistently, the potential of the 12 innermost monomers is used for the transport calculations, exploiting the approach described in [33], which allows for combining calculations of differently dimensioned systems for self-consistent field and transport calculations, respectively.

At first we consider a rotation that affects a single thiophene-thiophene bond only. The *p* conductivity of P3HT is governed by the states close to the valence-band maximum (VBM). They correspond to overlapping p_z orbitals of the thiophene rings that are perpendicular to the thiophene plane. Since the overlap of these p_z orbitals is directly affected by the torsion, one expects a strong decrease of the quantum conductance with increasing torsion angle, as indeed shown earlier by transfer integral calculations [13, 17, 18].

In fact, also the quantum conductance through single twisted thiophene-thiophene bonds calculated here is reduced with increasing twist angle, see blue curve in Fig. 5. There is a pronounced conductance minimum for square angles, where no delocalized π-bonds can be formed anymore (cf. Fig. 4b). In addition to the vanishing overlap of the carbon p_z-like orbitals directly at the defect, one observes in Fig. 4b a fragmentation of the highest occupied molecular orbital (HOMO) in the adjacency of the defect. Interestingly, the calculated conductance shows for twist angles up to around 60° only a moderate conductance drop to about 80 %.

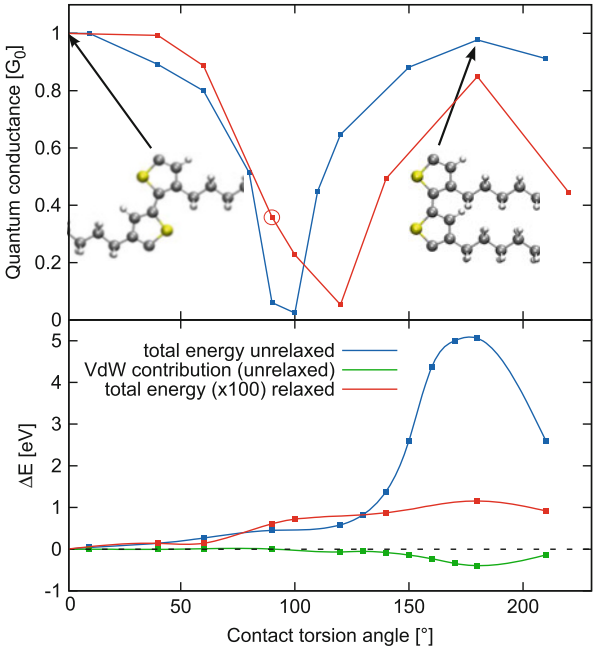

Fig. 5 *Top*: calculated conductance at the VBM through single twisted thiophene-thiophene bonds (*blue*) and configurations, where the total torsion angle around the polymer axis is realized by a sequence of twists obtained from structural relaxation (*red*). The respective geometries for zero and 180° rotation are shown as *insets*. The encircled data point corresponds to the configuration shown in Fig. 6. *Bottom*: total-energy increase due to the bond twisting for the case that only a single bond is twisted (*blue*) and for configurations where the torsion is realized by a sequence of twists obtained from structural relaxation (*red*). The dispersion energy contributions to the former case are shown in *green*

The calculated conductance vs. twist angle is not symmetric with respect to its minimum, since the corresponding torsion does not represent a symmetry transformation of the polymer, as illustrated by the 0° and 180° configurations shown in Fig. 5. Furthermore, the angles 140° and 220° are not equivalent as the polymer is slightly bent (cf. Fig. 2 in [38]).

The total energy as a function of the twist angle is shown by a blue line in the lower part of Fig. 5. For single bond twisting there is only a minor increase in energies for small torsion angles, suggesting that thermal activation may lead to corresponding geometry changes: The energy difference between the ideal polymer and the structure twisted by 10° (20°) amounts to 5 (37 meV). These torsion angles may thus be expected at room temperature if the chain motion is not strongly constrained otherwise. This is in accord with molecular dynamics simulations [39]. There is a steep increase of the total energy for torsion angles in excess of 150°. This is related to the steric repulsion of the hexyl side chains, which is only to a

small extent compensated by attractive van der Waals forces (green curve in Fig. 5), and efficiently prevents substantial rotations around single bonds.

The finding that only twists larger than about 60° have a measurable impact on the polymer conductance suggests that the overall conductance decrease will be reduced if not only a single bond is twisted, but if the total torsion angle around the polymer axis is realized by a sequence of twists. Moreover, such a sequence of rotations may be energetically more favorable than a single twisted bond. For this reason we also consider polymer geometries that result from the structural relaxations where the total torsion angle is fixed by the boundary conditions, but may be distributed among several thiophene-thiophene bonds. It is found that upon relaxation the hexyl side chains increase their mutual distance which leads to energetically far more favorable structures, see red curve (instead of the blue curve) in the lower part of Fig. 5. Also the quantum conductivity calculated for these relaxed structures differs from the corresponding curve for single bond twists, see upper part of Fig. 5. Not only the conductance drop is reduced and its onset occurs now for larger rotation angles, also the minimum of the transmission curve has shifted from nearly perpendicular to about 120°. This is a consequence of the nonlinear relation between conductance drop and bond twist. In case of a total torsion of 90° the maximum twist angle between two adjacent thiophene rings is 41° (cf. Fig. 6a). Hence, there is still some wave function delocalization along

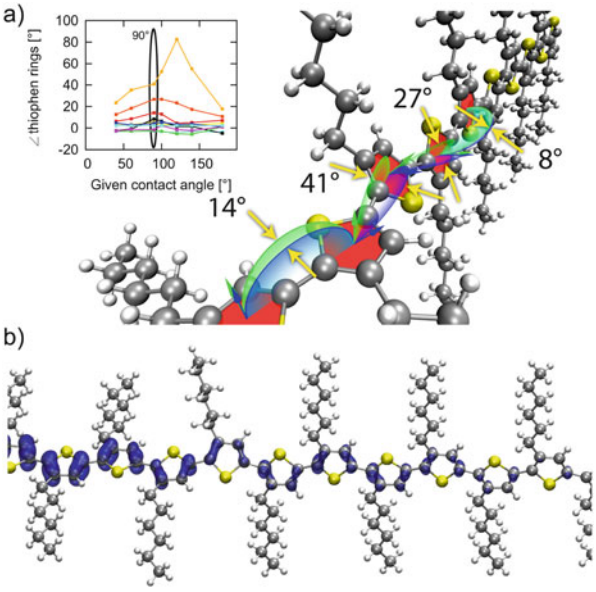

Fig. 6 (**a**) Atomic structure obtained upon structural relaxation for an overall torsion angle of 90° induced by the boundary conditions. The resulting twist angles for single bonds between thiophene rings are indicated. The data point belonging to the calculated quantum conductance for this configuration is highlighted in Fig. 5. The *inset* shows the twist angle distributions calculated here for various torsions. (**b**) Charge density isosurfaces indicate the HOMO for the structure above

the polymer direction. Only for total torsions as large as 120° where maximum twist angles of about 83° occur, the conductance is essentially quenched due to the vanishing overlap between the carbon *p* orbitals and a strongly fragmented HOMO.

We find the product of the transmission coefficients calculated for single twists to be a very rough approximation to the transmission through the complete torsional defect: The product of the transmission coefficients corresponding to the overall chain torsion of 90° realized by the structure shown in Fig. 6a for example is about twice as large as the transmission coefficient obtained from the solution of the complete scattering problem of this structure, cf. highlighted data point in Fig. 5. This may partially be related to the stronger fragmentation of the HOMO induced by an extended distortion pattern, cf. Figs. 4b and 6b. In case of single confined twists the reduced overlap between neighbouring thiophen orbitals limits the charge transfer, whereas the HOMO is interrupted for several monomers in case of the extended defect. Obviously, the transfer integral approach has to be applied with care to complex deformation patterns.

The present total-energy findings obtained for various torsion patterns indicate that the minimum energy configuration for a given torsion angle is realized by a sequence of single twists of similar amplitude, i.e., a helix configuration. However, the energy gain upon helix formation is small, of the order of a few meV, and the formation of such regular structures will in general be prevented by the surrounding P3HT matrix.

Polymer bending is a common defect for P3HT [40] that occurs along with torsions. In order to model this defect we analyze several folded P3HT chains. We characterize these foldings by their minimum curvature radius along the polymer chain. The starting configuration is structurally relaxed, where the atoms of the inner ten monomers (250 atoms) are free to move and the outer four monomers are kept frozen. This leads to polymer geometries such as shown in Fig. 7. The structures resulting for small curvatures are rather regular with straight and ordered hexyl side chains. With increasing curvature additional disorder including torsional defects is observed, see Fig. 7.

The inset in Fig. 7 shows the quantum conductance calculated for the relaxed geometries in dependence of their minimum curvature radii. Remarkably, the conductance is nearly unaffected by the structural deformations that have radii larger than about 17 Å. This can be rationalized in terms of the overlap between *p* orbitals of neighboring thiophene rings: While thiophene ring torsions may completely quench this overlap, chain bending leads to an overlap decrease/increase on opposite polymer sides. Additionally, we observe very efficient local relaxation mechanisms that smooth the polymer structure and prevent sharp kinks. The calculated conductance is quenched, however, for small curvature radii that also lead to bond twists caused by the structural relaxation in response to hexyl side chain related strain. For curvature radii smaller than 12 Å a similar effect on the calculated conductance is found as for twist angles larger than about 60°. The critical influence of the hexyl side chains onto the planarity of the backbone has already been pointed out in [36]. Similarly as observed for torsion patterns, a HOMO fragmentation is observed upon bending, cf. Fig. 7.

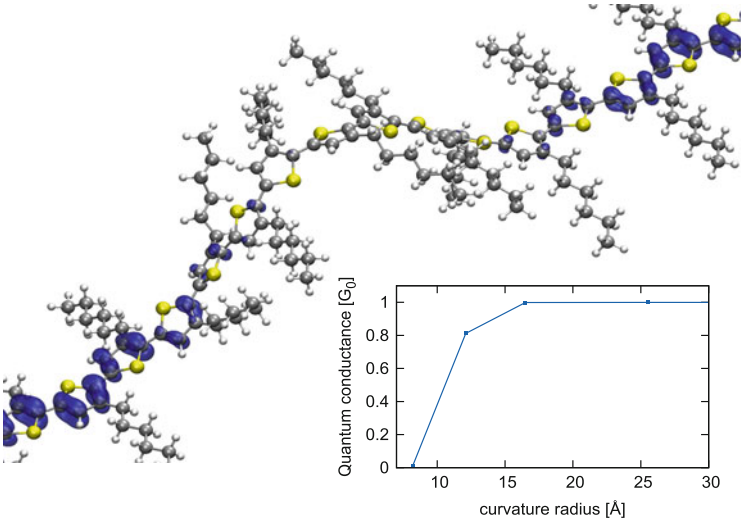

Fig. 7 Relaxed molecular structure with a minimum curvature radius of 8 Å. Charge density isosurfaces indicate the HOMO. The calculated quantum conductance for structures with different curvature radii are shown as *inset*

Crystalline regioregular (rr)-HT-P3HT is of particular interest for organic semiconductor devices due to its large carrier mobility of up to 0.1 $cm^2/(Vs)$ [41]. Here the identifier HT indicates the head-tail coupling between two thiophene rings where H denotes the second and T the fifth position on the ring, with numeration starting at the sulfur atom as shown in Fig. 3. In order to assess the influence of isomer defects on the (rr)-HT-P3HT transport properties, the intrachain scattering along a defective polymer is calculated, where HH and TT coupling instead of HT occurs, according to a replacement of a hexyl side chain, see Fig. 3. Ideal rr-HT-P3HT segments serve as contacts to the isomer defect. Additional HT coupled P3HT segments in the vicinity of the defect are included in the scattering region, in order to allow for a realistic modeling of the geometrical and electronic environment of the defect embedded in the polymer.

The calculated quantum conductance of the isomer defect (red) is compared with corresponding calculations for the ideal P3HT chain (blue) in Fig. 8 rhs. The data for the ideal P3HT chain can be obtained by simply counting the number of bands at a given energy (cf. blue band structure in Fig. 8 lhs). As the holes will almost exclusively move at the Fermi edge, we find only one conducting band which results in a maximum quantum conductance of 1 G_0.

Close to the Fermi edge a small conductance reduction is caused by the defect. Stronger defect induced drops occur, however, for energies about 2.3 eV below the VBM, cf. Fig. 8. They will barely affect the actual electron transport that is governed by charge carrier close to the VBM. The physical origin for the sharp drop around -2.3 eV is a strong wave function localization at the corresponding energy, cf. [33].

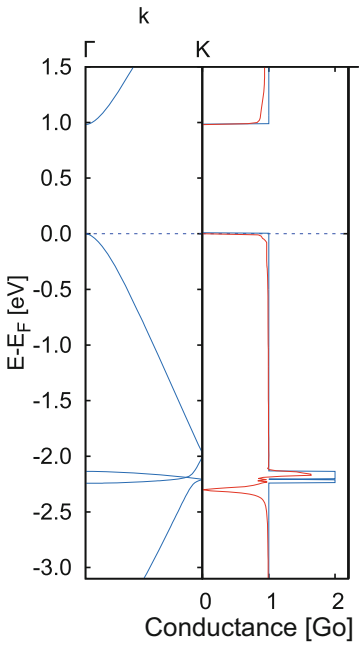

Fig. 8 *Left*: band structure of rr-HT-P3HT along the chain direction. *Right*: quantum conductance for rr-HT-P3HT (*blue*) in comparison to the calculations for the single isomer defect shown in Fig. 3 (*red*)

The all in all minor transport changes induced by the isomer defect confirm that the P3HT transport properties are determined by the thiophene rings rather than the hexyl side chains. The present results indicate that the conductance of (rr)-HT-P3HT is surprisingly robust with respect to the occurrence of single and repeated isomer defects. However, such disorder will affect the bulk morphology and might therefore have some influence on the performance of the polymer in electronics applications [42].

Oxygen is used as *p*-dopant in organic semiconductors where it forms a reversible charge transfer complex [43–45], but may also be present unintentionally due to the exposure to ambient atmosphere and aging. Chemical reactions of O_2 and P3HT may result in a covalent bonding between oxygen and carbon as well as sulfur [46]. The P3HT degradation upon exposure to oxygen [47, 48] decreases the charge carrier mobility [45]. Thereby differences are observed between the effect of oxygen and ozone [49]. Experimentally, the formation of S-O and C-O bond containing species upon P3HT exposure to air was detected [50]. In the present work we focus on the energetically most favored S and C structures identified in recent calculations [37], cf. Fig. 9. It can be seen that both oxygen defects slightly repel the nearest hexyl side chain and that the C defect slightly distorts the thiophene ring.

In order to calculate the influence of these two O defects on the P3HT intrachain transport we proceed similarly as above, i.e., we use ideal rr-HT-P3HT contacts which sandwich a scatter region of 12 monomers including the defect. The scatter region has a length of 47 Å. The calculated quantum conductance for the two defects is shown in Fig. 10 along with the results for the ideal P3HT chain. Obviously, the

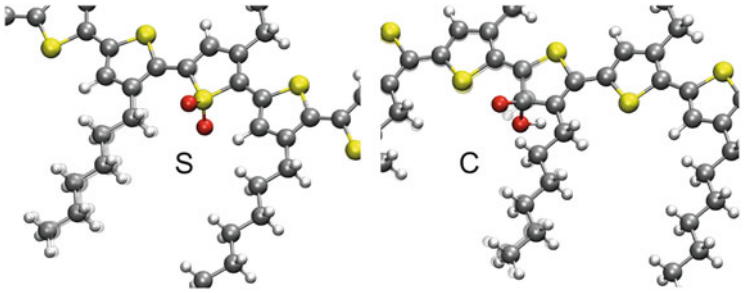

Fig. 9 Calculated relaxed geometries of two oxygen impurity configurations S and C in P3HT. The *shaded atoms* indicate the oxidation induced structure changes

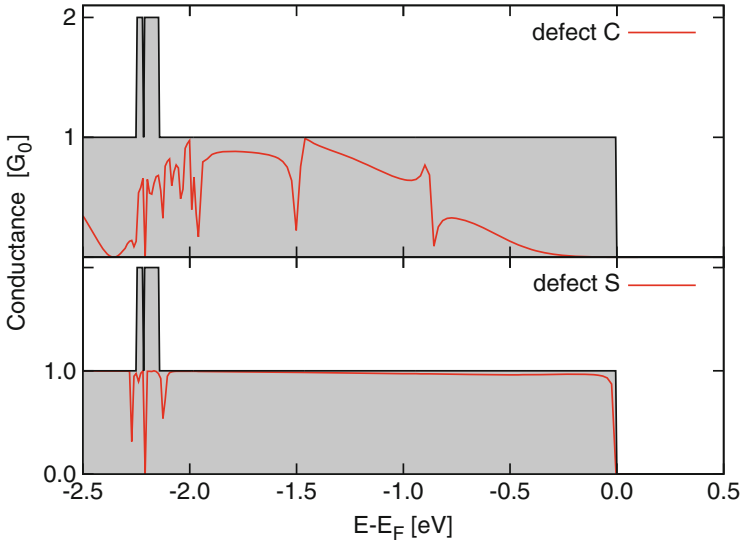

Fig. 10 Calculated quantum conductance through defect S and C, cf. Fig. 9. The *shaded region* is the maximum possible quantum conductance for rr-HT-P3HT

two defects differ strongly in their influence on the polymer conductance. The S defect barely influences the transport even for energies far below the VBM. Only conduction channels at around −2.2 eV are broken. This is in marked contrast to the C defect, which nearly quenches the hole transport up to nearly 1 eV below the VBM.

In order to understand the different transport properties of the two defects we analyze their influence on the electronic density of states (DOS), cf. [33]. It is found that, apart from minor energy shifts, the DOS of S nearly coincides with the respective calculations for the ideal polymer. Only for energies below −2 eV additional, oxygen-localized *p* states appear. Stronger deviations occur in case of C, where the complete valence band DOS is modified and additional oxygen *p* states

show up at the VBM. This different behaviour is expected: The P3HT valence band is formed by p orbitals of the conjugated chain system which are little influenced by the adsorption of oxygen to the sulfur. However, oxidation of a thiophene group carbon directly affects the conjugated electron system and thus has a major influence on the transport in the valence band.

4 Conclusions

A scattering approach based on the self-consistent DFT electronic structure is employed to study the on-chain quantum conductance of P3HT. The influence of defects on the intrachain transport is highly specific. Large torsion angles hinder the formation of a delocalized π electron system and, thus, the transport along the polymer direction while the chain bending has a considerably smaller effect on the conductance. Structural relaxation tends to recover geometries with favorable electron transport properties. The calculations performed for complex distortion patterns show that their conductivity cannot simply be broken down into conductivity drops related the disturbed interaction of directly neighboring molecular segments. P3HT oxidation is found to affect the intrachain transmission strongly, when thiophene group C atoms are attacked, while sulfur oxidation barely modifies the transmission. Also the conductance drop due to isomer defects in the chain is negligible.

Acknowledgements The calculations were done using grants of computer time from the Höchstleistungs-Rechenzentrum Stuttgart (HLRS) and the Paderborn Center for Parallel Computing (PC^2). The Deutsche Forschungsgemeinschaft (FOR1700, FOR1405, SF-TRR142, SCHM 1361/21) is acknowledged for financial support.

References

1. Dang, M.T., Hirsch, L., Wantz, G.: Adv. Mater. **23**(31), 3597 (2011). doi:10.1002/adma.201100792
2. Vukmirovic, N., Wang, L.W.: J. Phys. Chem. B **113**(2), 409 (2009). doi:10.1021/jp808360y
3. McMahon, D.P., Troisi, A.: ChemPhysChem **11**(10), 2067 (2010). doi:10.1002/cphc.201000182
4. Bjorgaard, J.A., Köse, M.E.: J. Phys. Chem. A **117**(18), 3869 (2013). doi:10.1021/jp401521j
5. Vukmirović, N., Wang, L.W.: J. Chem. Phys. **134**(9), (2011). doi:10.1063/1.3560956. http://scitation.aip.org/content/aip/journal/jcp/134/9/10.1063/1.3560956
6. Beenken, W.J.D., Pullerits, T.: J. Phys. Chem. B **108**(20), 6164 (2004). doi:10.1021/jp037332l
7. Kline, R.J., McGehee, M.D.: J. Macromol. Sci. Polym. Rev. **46**(1), 27 (2006). doi:10.1080/15321790500471194
8. Coropceanu, V., Cornil, J., da Silva Filho, D.A, Olivier, Y., Silbey, R., Brédas, J.L.: Chem. Rev. **107**(4), 926 (2007). doi:10.1021/cr050140x
9. Nelson, J., Kwiatkowski, J.J., Kirkpatrick, J., Frost, J.M.: Acc. Chem. Res. **42**(11), 1768 (2009). doi:10.1021/ar900119f

10. Pingel, P., Zen, A., Abellón, R.D., Grozema, F.C., Siebbeles, L.D., Neher, D.: Adv. Funct. Mater. **20**(14), 2286 (2010). doi:10.1002/adfm.200902273
11. Kline, R.J.., McGehee, M.D., Kadnikova, E.N., Liu, J., Fréchet, J.M.J., Toney, M.F.: Macromolecules **38**(8), 3312 (2005). doi:10.1021/ma047415f
12. Crossland, E.J.W., Tremel, K., Fischer, F., Rahimi, K., Reiter, G., Steiner, U., Ludwigs, S.: Adv. Mater. **24**(6), 839 (2012). doi:10.1002/adma.201104284
13. Lan, Y.K., Huang, C.I.: J. Phys. Chem. B **112**(47), 14857 (2008). doi:10.1021/jp806967x
14. Lan, Y.K., Huang, C.I.: J. Phys. Chem. B **113**(44), 14555 (2009). doi:10.1021/jp904841j
15. Noriega, R., Rivnay, J., Vandewal, K., Koch, F.P.V., Stingelin, N., Smith, P., Toney, M.F., Salleo, A.: Nat. Mater. **12**(11), 1038 (2013). doi:10.1038/nmat3722
16. Darling, S.B., Sternberg, M.: J. Phys. Chem. B **113**(18), 6215 (2009). doi:10.1021/jp808045j
17. Grozema, F.C., van Duijnen, P.Th., Berlin, Y.A., Ratner, M.A., Siebbeles, L.D.A.: J. Phys. Chem. B **106**(32), 7791 (2002). doi:10.1021/jp021114v
18. Darling, S.B.: J. Phys. Chem. B **112**(30), 8891 (2008). doi:10.1021/jp8017919
19. Jackson, N.E., Savoie, B.M., Kohlstedt, K.L., Marks, T.J., Chen, L.X., Ratner, M.A.: Macromolecules **47**(3), 987 (2014). doi:10.1021/ma4023923
20. Datta, S.: Electronic Transport in Mesoscopic Systems. Cambridge Studies in Semiconductor Physics and Microelectronic Engineering, vol. 3, 8th edn. Cambridge University Press, Cambridge (2009)
21. Alessandro, T.: Adv. Polym. Sci. **223**, 259 (2010)
22. Giannozzi, P., Baroni, S., Bonini, N., Calandra, M., Car, R., Cavazzoni, C., Ceresoli, D., Chiarotti, G.L., Cococcioni, M., Dabo, I., Dal Corso, A., Gironcoli, S.D., Fabris, S., Fratesi, G., Gebauer, R., Gerstmann, U., Gougoussis, C., Kokalj, A., Lazzeri, M., Martin-Samos, L., Marzari, N., Mauri, F., Mazzarello, R., Paolini, S., Pasquarello, A., Paulatto, L., Sbraccia, C., Scandolo, S., Sclauzero, G., Seitsonen, A.P., Smogunov, A., Umari, P., Wentzcovitch, R.M.: J. Phys. Condens. Mat. **21**(39), 395502 (2009). doi:10.1088/0953-8984/21/39/395502
23. Vanderbilt, D., Phys. Rev. B **41**(11), 7892 (1990). doi:10.1103/PhysRevB.41.7892
24. Kleinman, L., Bylander, D.: Phys. Rev. Lett. **48**(20), 1425 (1982). doi:10.1103/PhysRevLett.48.1425
25. Perdew, J., Burke, K., Ernzerhof, M.: Phys. Rev. Lett. **77**(18), 3865 (1996). doi:10.1103/PhysRevLett.77.3865
26. Perdew, J., Burke, K., Ernzerhof, M.: Phys. Rev. Lett. **78**(7), 1396 (1997). doi:10.1103/PhysRevLett.78.1396
27. London, F.: Z. Phys. Chem. Abt. B **11**, 222 (1930)
28. Ortmann, F., Schmidt, W.G., Bechstedt, F.: Phys. Rev. Lett. **95**(18), 186101 (2005). doi:10.1103/PhysRevLett.95.186101
29. Grimme, S.: J. Comput. Chem. **27**(15), 1787 (2006). doi:10.1002/jcc.20495
30. Choi, H.J., Ihm, J., Phys. Rev. B **59**(3), 2267 (1999). doi:10.1103/PhysRevB.59.2267
31. Smogunov, A., Dal Corso, A., Tosatti, E.: Phys. Rev. B **70**(4), 045417 (2004). doi:10.1103/PhysRevB.70.045417
32. Sclauzero, G., Dal Corso, A., Smogunov, A.: Phys. Rev. B **85**(16), 165411 (2012). doi:10.1103/PhysRevB.85.165411
33. Lücke, A., Schmidt, W.G., Rauls, E., Ortmann, F., Gerstmann, U.: J. Phys. Chem. B **119**, 6481 (2015)
34. Grozema, F.C., Siebbeles, L.D.A.: J. Phys. Chem. Lett. **2**(23), 2951 (2011). doi:10.1021/jz201229a
35. Salaneck, W.R., Inganäs, O., Thémans, B., Nilsson, J.O., Sjögren, B., Österholm, J.E., Brédas, J.L., Svensson, S.: J. Chem. Phys. **89**(8), 4613 (1988). doi:10.1063/1.454802
36. Dkhissi, A., Ouhib, F., Chaalane, A., Hiorns, R.C., Dagron-Lartigau, C., Iratcabal, P., Desbrieres, J., Pouchan, C.: Phys. Chem. Chem. Phys. **14**(16), 5613 (2012). doi:10.1039/c2cp40170c
37. Volonakis, G., Tsetseris, L., Logothetidis, S.: Phys. Chem. Chem. Phys. **16**(46), 25557 (2014). doi:10.1039/c4cp03203a
38. Colle, R., Grosso, G., Ronzani, A., Zicovich-Wilson, C.M.: Phys. Status Solidi B **248**(6), 1360 (2011). doi:10.1002/pssb.201046429

39. Alexiadis, O., Mavrantzas, V.G.: Macromolecules **46**(6), 2450 (2013). doi:10.1021/ma302211g
40. Chang, J.F., Clark, J., Zhao, N., Sirringhaus, H., Breiby, D., Andreasen, J., Nielsen, M., Giles, M., Heeney, M., McCulloch, I.: Phys. Rev. B **74**(11) (2006). doi:10.1103/PhysRevB.74.115318
41. Sirringhaus, H., Brown, P.J., Friend, R.H., Nielsen, M.M., Bechgaard, K., Langeveld-Voss, B.M.W., Spiering, A.J.H., Janssen, R.A.J., Meijer, E.W., Herwig, P., Leeuw, D.M.D.: Nature **401**(6754), 685 (1999). doi:10.1038/44359
42. McMahon, D.P., Cheung, D.L., Goris, L., Dacuña, J., Salleo, A., Troisi, A.: J. Phys. Chem. C **115**(39), 19386 (2011). doi:10.1021/jp207026s
43. Lüer, L., Egelhaaf, H.J., Oelkrug, D., Cerullo, G., Lanzani, G., Huisman, B.H., Leeuw, D.D.: Curr. Trends Cryst. Org. Semicond. Growth Model. Fundam. Prop. **5**(1–3), 83 (2004). doi:10.1016/j.orgel.2003.12.005. http://www.sciencedirect.com/science/article/pii/S1566119904000059
44. Liao, H.H., Yang, C.M., Liu, C.C., Horng, S.F., Meng, H.F., Shy, J.T.: J. Appl. Phys. **103**(10), 104506 (2008). doi:10.1063/1.2917419
45. Schafferhans, J., Baumann, A., Wagenpfahl, A., Deibel, C., Dyakonov, V.: Org. Electron. **11**(10), 1693 (2010). doi:10.1016/j.orgel.2010.07.016. http://www.sciencedirect.com/science/article/pii/S1566119910002466
46. Seemann, A., Sauermann, T., Lungenschmied, C., Armbruster, O., Bauer, S., Egelhaaf, H.J., Hauch, J.: Org. Photovolt. Dye Sensitized Sol. Cells **85**(6), 1238 (2011). doi:10.1016/j.solener.2010.09.007. http://www.sciencedirect.com/science/article/pii/S0038092X10002999
47. Sirringhaus, H.: Adv. Mater. **21**(38–39), 3859 (2009). doi:10.1002/adma.200901136
48. Grossiord, N., Kroon, J.M., Andriessen, R., Blom, P.W.M.: Org. Electron. **13**(3), 432 (2012). doi:10.1016/j.orgel.2011.11.027. http://www.sciencedirect.com/science/article/pii/S1566119911004046
49. Chabinyc, M.L., Street, R.A., Northrup, J.E.: Appl. Phys. Lett. **90**(12), 123508 (2007). doi:10.1063/1.2715445
50. Norrman, K., Madsen, M.V., Gevorgyan, S.A., Krebs, F.C.: J. Am. Chem. Soc. **132**(47), 16883 (2010). doi:10.1021/ja106299g